

## Hollow Nanoparticles of Metal Oxides and Sulfides: Fast Preparation via Laser Ablation in Liquid

K. Y. Niu,<sup>†</sup> J. Yang,<sup>†</sup> S. A. Kulinich,<sup>‡,§</sup> J. Sun,<sup>†</sup> and X. W. Du<sup>\*†</sup><sup>†</sup>School of Materials Science and Engineering, Tianjin University, Tianjin 300072, PR China,<sup>‡</sup>Department of Chemistry, University of British Columbia, Vancouver, BC, Canada V6T 1Z1, and<sup>§</sup>Department of Applied Sciences, University of Quebec, Saguenay, PQ, Canada G7H 2B1

Received August 19, 2010. Revised Manuscript Received October 4, 2010

In this work, diverse hollow nanoparticles of metal oxides and sulfides were prepared by simply laser ablating metal targets in properly chosen liquids. The Kirkendall voiding and the selective heating with an infrared laser were shown to work as two independent mechanisms for the formation of such hollow nanoparticles in only one- or two-step synthesis approaches. One of the prepared materials, ZnS hollow nanoparticles, showed high performance in gas sensing. The simple, fast, inexpensive technique that is proposed demonstrates very promising perspectives.

## Introduction

The special structure of nanomaterials gives rise to their amazing properties. As a unique nanostructure, hollow nanoparticles (HNPs) exhibit many outstanding features such as low density, a high surface-to-volume ratio, and the effect of void space and have found applications in many fields such as Li ion batteries,<sup>1–3</sup> catalysis,<sup>4,5</sup> gas sensing,<sup>6,7</sup> and drug/DNA delivery.<sup>8,9</sup> A large number of methods have been developed to synthesize various HNPs, with the majority being classified as hard templating,<sup>10–13</sup> soft templating,<sup>14,15</sup> template-free,<sup>3,16</sup> and sacrificial templating approaches.<sup>2,17</sup> So far, all HNPs have been produced solely through chemical routes, which normally involve several steps and often require copious amounts of numerous chemicals. Most prepared nanostructures were larger than 100 nm, and smaller HNPs were seldom reported.<sup>18–20</sup> Therefore, new synthesis

routes to preparing HNPs with different sizes and chemical compositions (at reasonable costs) are still highly anticipated.

Kirkendall voiding is often employed as a final step when preparing HNPs.<sup>17,18,20</sup> During the oxidation of a metallic particle, if its metal core diffuses rapidly outward while the oxidizer diffuses slowly inward, then the process is referred to as the Kirkendall effect and can result in an HNP.<sup>17,18</sup> Therefore, the Kirkendall effect is applicable only to metals with high diffusion coefficients in their oxide, sulfide, or selenide shells,<sup>17</sup> for instance, Co,<sup>18</sup> Ni,<sup>19</sup> Zn,<sup>21</sup> Fe,<sup>22</sup> and Cu.<sup>23</sup> A good example of a Kirkendall-mechanism-mediated synthesis route to preparing uniform, ultrafine HNPs is the one-pot approach reported by the Alivisatos group.<sup>18</sup> As a first step, colloidal Co nanoparticles were chemically formed, after which either an organic solution of chalcogene (S or Se) was injected or an O<sub>2</sub>/Ar gas flow was blown through the heated solution.<sup>18</sup> Correspondingly, cobalt sulfide, selenide, or oxide HNPs were formed upon Kirkendall voiding at high temperatures (normally ~182 °C). Depending on the size and chemical composition, it took from several seconds to about 30–210 min to convert metal nanoparticles completely into HNPs.<sup>18</sup>

Here, we demonstrate that a one-pot (but also one-step) process can be realized by applying a laser-involved process in which metal nanoparticles first form and then transform in situ into HNPs via reactions with a liquid medium and Kirkendall voiding. Thus, both steps in the Alivisatos approach<sup>18</sup> (i.e., nanoparticle formation and Kirkendall voiding) can be combined into one step. The technique proposed is very versatile and allowed us to prepare diverse HNPs of metal oxides and sulfides, including some that have not been reported (e.g., MgO and PbS HNPs).

Laser ablation in liquid (LAL) is well known as a simple and conventional technique for the preparation of colloid nanoparticles.<sup>24–27</sup> A large number of metal nanoparticles were

\*Corresponding author. E-mail: xwdu@tju.edu.cn.

- (1) Lou, X. W.; Archer, L. A. *Adv. Mater.* **2008**, *20*, 1853–1858.
- (2) Lou, X. W.; Archer, L. A.; Yang, Z. C. *Adv. Mater.* **2008**, *20*, 3987–4019.
- (3) Lou, X. W.; Wang, Y.; Yuan, C. L.; Lee, J. Y.; Archer, L. A. *Adv. Mater.* **2006**, *18*, 2325–2329.
- (4) Kim, S. W.; Kim, M.; Lee, W. Y.; Hyeon, T. *J. Am. Chem. Soc.* **2002**, *124*, 7642–7643.
- (5) Liang, H. P.; Zhang, H. M.; Hu, J. S.; Guo, Y. G.; Wan, L. J.; Bai, C. L. *Angew. Chem., Int. Ed.* **2004**, *43*, 1540–1543.
- (6) Martinez, C. J.; Hockey, B.; Montgomery, C. B.; Semancik, S. *Langmuir* **2005**, *21*, 7937–7944.
- (7) Zhang, H. G.; Zhu, Q. S.; Zhang, Y.; Wang, Y.; Zhao, L.; Yu, B. *Adv. Funct. Mater.* **2007**, *17*, 2766–2771.
- (8) Zhu, Y. F.; Shi, J. L.; Shen, W. H.; Dong, X. P.; Feng, J. W.; Ruan, M. L.; Li, Y. S. *Angew. Chem., Int. Ed.* **2005**, *44*, 5083–5087.
- (9) Cai, Y. R.; Pan, H. H.; Xu, X. R.; Hu, Q. H.; Li, L.; Tang, R. K. *Chem. Mater.* **2007**, *19*, 3081–3083.
- (10) Caruso, F.; Caruso, R. A.; Mohwald, H. *Science* **1998**, *282*, 1111–1114.
- (11) Jiang, P.; Bertone, J. F.; Colvin, V. L. *Science* **2001**, *291*, 453–457.
- (12) Suarez, F. J.; Sevilla, M.; Alvarez, S.; Valdes-Solis, T.; Furtres, A. B. *Chem. Mater.* **2007**, *19*, 3096–3098.
- (13) Arnal, P. M.; Weidenthaler, C.; Schuth, F. *Chem. Mater.* **2006**, *18*, 2733–2739.
- (14) Buchold, D. H. M.; Feldmann, C. *Nano Lett.* **2007**, *7*, 3489–3492.
- (15) Wu, C. Z.; Xie, Y.; Lei, L. Y.; Hu, S. Q.; OuYang, C. Z. *Adv. Mater.* **2006**, *18*, 1727–1732.
- (16) Zeng, H. C. *Curr. Nanosci.* **2007**, *3*, 177–181.
- (17) Fan, H. J.; Gosele, U.; Zacharias, M. *Small* **2007**, *3*, 1660–1671.
- (18) Yin, Y. D.; Rioux, R. M.; Erdonmez, C. K.; Hughes, S.; Somorjai, G. A.; Alivisatos, A. P. *Science* **2004**, *304*, 711–714.
- (19) Latham, A. H.; Williams, M. E. *Langmuir* **2008**, *24*, 14195–14202.
- (20) Railsback, J. G.; Johnston-Peck, A. C.; Wang, J. W.; Tracy, J. B. *ACS Nano* **2010**, *4*, 1913–1920.

(21) Nakamura, R.; Lee, J. G.; Tokozakura, D.; Mori, H.; Nakajima, H. *Mater. Lett.* **2007**, *61*, 1060–1063.

(22) Wang, C. M.; Baer, D. R.; Thomas, L. E.; Amonette, J. E.; Antony, J.; Qiang, Y.; Duscher, G. J. *Appl. Phys.* **2005**, *98*, 094308.

(23) Nakamura, R.; Tokozakura, D.; Nakajima, H.; Lee, J. G.; Mori, H. *J. Appl. Phys.* **2007**, *101*, 074303.

(24) Sun, J.; Hu, S. L.; Du, X. W.; Lei, Y. W.; Jiang, L. *Appl. Phys. Lett.* **2006**, *89*, 183115.

(25) Lin, F.; Yang, J.; Lu, S. H.; Niu, K. Y.; Liu, Y.; Sun, J.; Du, X. W. *J. Mater. Chem.* **2010**, *20*, 1103–1106.

**Table 1. Experimental Details and Products after One-Step Laser Treatment**

material system	target	liquid medium	volume ratio	product
Zn/S	Zn	$\beta$ -mercaptoethanol	N/A	HNPs
Pb/S	Pb	mercaptoacetic acid	N/A	HNPs
Pb/S	Pb	dodecyl mercaptan/ <i>n</i> -hexane	1:5	core/shell NSs
Mg/O	Mg	<i>n</i> -hexane/ethanol	1:0/5:1/0:1	MNPs/HNPs/MgO NCs <sup>a</sup>
Cu/O	Cu	water/ethanol	5:1	HNPs
Co/O	Co	water/ethanol	10:1	HNPs
Fe/O	Fe	water/ethanol	5:2	core/hollow shell NSs
Zn/O	Zn	water/ethanol	1:10/1:8/1:6	core/shell NSs
Ti/O	Ti	water/ethanol	1:3/1:5	core/shell NSs

<sup>a</sup>Note: MNPs (Mg nanoparticles), HNPs (hollow nanoparticles), NCs (nanocubes), and NSs (nanospheres).

reported to be synthesized through laser irradiation of metal targets in liquid.<sup>27</sup> Yang et al. applied this technique to produce Si (or Ag) nanoparticles in liquid, which were then electrochemically deposited on polymer templates to produce hollow microstructures.<sup>28</sup> The direct synthesis of HNPs by solely using the LAL was not proposed or well described thus far.

Recently, we reported on the controllable synthesis of diverse nanostructures through ablating metal targets in reactive liquids with a long-pulse-width laser. Surface reactions of metal nanodroplets were demonstrated to play a key role in controlling the product morphology, thus opening a new avenue to the preparation of diverse nanostructures, including HNPs, via the LAL.<sup>29</sup> In the present work, we show that HNPs of numerous metal oxides and sulfides can be efficiently prepared by employing the LAL as a one-step (or two-step), one-pot technique. The laser-generated metal nanodroplets can convert into HNPs in situ through the Kirkendall effect, provided that appropriate metal targets and reactive liquid media are selected and experimental conditions are properly adjusted. We also show that laser irradiation can be applied to certain metal core/shell structures to vaporize their core selectively and convert them into HNPs. This treatment can be used as a second step in core/shell systems where Kirkendall voiding cannot be completed after one laser pulse. It can also be applied to prepare hollow nanostructures from appropriate core/shell structures synthesized through other approaches. The prepared HNPs are very small and have close to regular spherical shape, good dispersibility, and attractive properties. The results suggest that laser ablation is a versatile and promising technique for preparing (diverse) high-quality HNPs.

### Experimental Procedures

**Materials.** Zn, Mg, Fe, Co, Ni, Cu, Pb, or Ti targets (5 mm thick, purity quotient 99.99%) were ablated with a millisecond-pulsed Nd:YAG laser (1064 nm) in appropriate liquids with a volume of 20 mL and a depth of 5 mm. The compositions of the liquid media used were chosen and adjusted for each target and can be found in Table 1. The laser power density, pulse width, and frequency used in the experiments were  $10^6$  W/cm<sup>2</sup>, 0.6 ms, and 1 Hz, respectively, and the irradiation time was 5 min for all first-step laser treatments. Different spots on the target surface were ablated during each laser pulse by rotating the target at about 120 rpm. After laser ablation, the suspension was centrifuged (at 11 000 rpm) and the precipitate was further washed with ethanol and dried at 60 °C. This allowed us to evaluate the product yield, which was on the order of tens of mg/h, varying for different material systems. For the selective laser vaporization treatment,

Zn/ZnO, Ti/TiO<sub>2</sub>, and Pb/PbS core/shell nanospheres were first produced by the above first-step laser treatment, after which the metal target was removed from the liquid medium and the remaining suspension was further laser ablated (as a second step) for another 20 min. The same laser parameters and magnetic stirring of the solution were applied during this stage.

**Measurements and Analysis.** The product morphology was determined by an FEI Technai G2 F20 TEM equipped with a field-emission gun, and the composition was analyzed by an Oxford INCA energy-dispersive X-ray spectroscopy module attached to the TEM. The phase structure was investigated by using a Rigaku D/max 2500v/pc X-ray diffractometer. To fabricate a gas-sensing device, ZnS HNPs were mixed with terpineol to form a cream and then coated on a ceramic (Al<sub>2</sub>O<sub>3</sub>) tube with two golden electrodes at each end. The tube with ZnS HNPs was sintered at 300 °C, after which electrical contacts were made by attaching two platinum wires to the electrodes. Gas-sensing measurements were made in an HLGS-01 dynamic gas-sensing measurement system (Harbin University of Science and Technology, Harbin, China). Magnetic properties were detected in a Physical Property Measurement System (PPMS-9T, Quantum Design Co.).

### Results and Discussion

To examine the occurrence of the Kirkendall effect in the LAL experiments, we chose the following six material systems: Zn/S, Pb/S, Mg/O, Cu/O, Co/O, and Fe/O. Among these, the Zn/S, Pb/S, Cu/O, Co/O, and Fe/O systems had been previously reported as those where the Kirkendall effect takes place.<sup>19,21,22,30,31</sup> The Mg/O system, which had not been investigated before, was taken as a potential Kirkendall-effect system because of the smaller radius and larger diffusion coefficient of Mg ions compared to those of oxygen.<sup>32</sup> Upon carefully choosing and adjusting proper liquid media (Table 1), HNPs were obtained in the Zn/S, Pb/S, Mg/O, Cu/O, and Co/O systems (Figure 1a–e). As for the Fe/O system, core/shell nanostructures with apparent gaps between the core and shell were found (Figure 1f), implying somewhat slower void formation during laser irradiation.

Detailed characterization of the HNPs was performed by using TEM and XRD/EDS. The results in Figure 2 (Supporting Information Figure S1) show that the ZnS (~20 nm), MgO (~15 nm), and CoO (~50 nm) HNPs are polycrystalline whereas the CuO (~10 nm) and PbS (~30 nm) HNPs are single-crystalline (Figures 2a–e and S1a–e). As for the core/shell nanostructures obtained in the Fe/O system, the core and shell were found to be composed of Fe and Fe<sub>x</sub>O<sub>y</sub>, respectively (Figures 2f and S1f).

Laser ablation of solid targets in liquid has been commonly used to produce nanoparticles.<sup>24–27</sup> Our experiments demonstrate,

(26) Hu, S. L.; Niu, K. Y.; Sun, J.; Zhao, N. Q.; Du, X. W. *J. Mater. Chem.* **2009**, *19*, 484–488.

(27) Yang, G. W. *Prog. Mater. Sci.* **2007**, *52*, 648–698.

(28) Yang, S. K.; Cai, W. P.; Yang, J. L.; Zeng, H. B. *Langmuir* **2009**, *25*, 8287–8291.

(29) Niu, K. Y.; Yang, J.; Kulinich, S. A.; Sun, J.; Li, H.; Du, X. W. *J. Am. Chem. Soc.* **2010**, *132*, 9814–9819.

(30) Shao, H. F.; Qian, X. F.; Zhu, Z. K. *J. Solid State Chem.* **2005**, *178*, 3522–3528.

(31) Wang, Y. L.; Cai, L.; Xia, Y. N. *Adv. Mater.* **2005**, *17*, 473–477.

(32) Kooi, B. J.; Palasantzas, G.; De Hosson, J. T. M. *Appl. Phys. Lett.* **2006**, *89*, 161914.

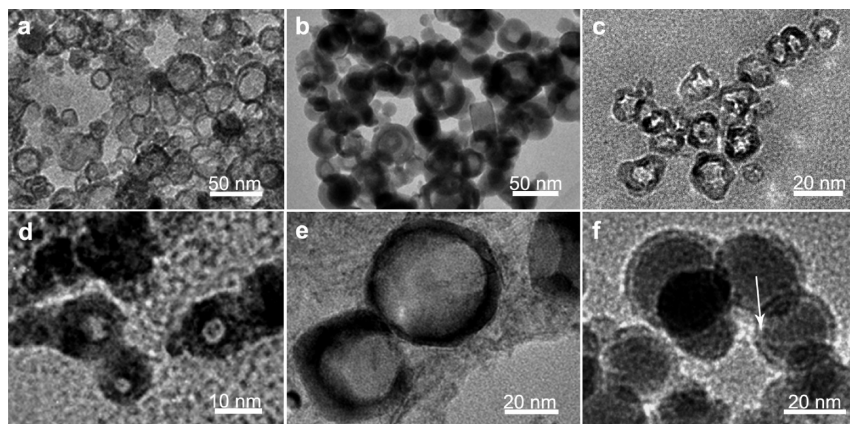


**Figure 1.** Transmission electron microscopy (TEM) images of HNPs prepared by one-step laser treatment. (a) ZnS, (b) PbS, (c) MgO, (d) CuO, and (e) CoO. (f) Fe/Fe<sub>x</sub>O<sub>y</sub> core/hollow shell nanospheres. The arrow indicates a gap between a metal core and an oxide shell.

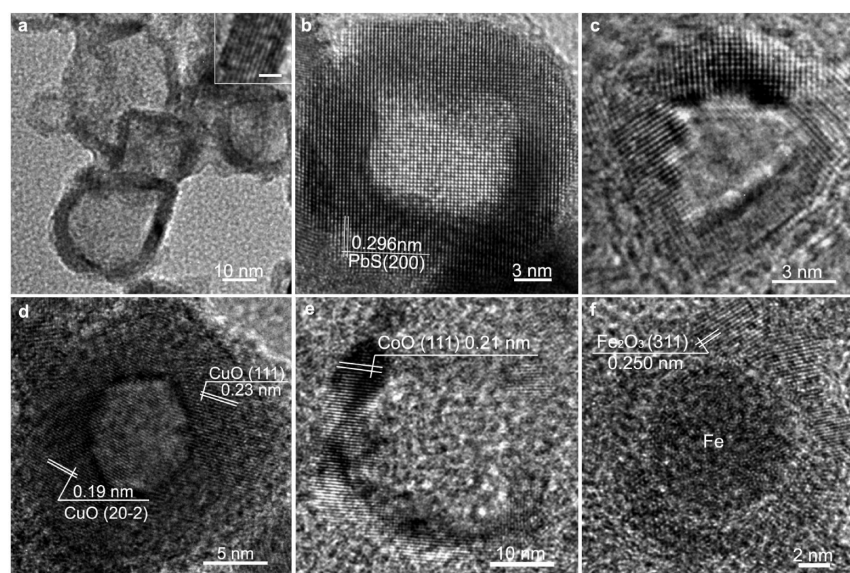


**Figure 2.** High-resolution TEM images of the as-produced hollow nanospheres. (a) ZnS HNPs, (b) PbS HNP, (c) MgO HNP, (d) CuO HNP, (e) CoO HNP, and (f) Fe/Fe<sub>x</sub>O<sub>y</sub> core/hollow shell nanosphere. The scale bar in the inset of image a indicates 1 nm.

for the first time, the possibility of preparing hollow nanostructures with this technique. There are two findings to support the hypothesis that the Kirkendall effect is responsible for the formation of the nanostructures presented in Figures 1 and 2. First, the high cooling rates, which are well known for the LAL process,<sup>27</sup> quenched intermediate states in the formation of ZnS HNPs, and such particles could be found as a small fraction in the main product. From those intermediate products, we could distinguish the Kirkendall voiding, appearance of diffusing bridges and surface spreading, and finally the formation of HNPs (Figure 3a–e).<sup>17,18,33</sup> The gap observed between the Fe cores and oxide shells (Figures 1f and 2f) is also an evident characteristic of the Kirkendall process.

The preparation of the MgO HNPs is the second argument in favor of the Kirkendall process. We assumed that, even for highly reactive metal Mg, if Mg/MgO core/shell nanostructures (with a proper shell thickness) formed during laser ablation then they could transform into MgO HNPs through Kirkendall voiding during a cooling stage following each laser pulse. Three different liquid media were tested in the Mg/O system, with the oxidizing

potential varied from low (*n*-hexane) to medium (*n*-hexane/ethanol) to high (ethanol). As the Mg target was ablated in these liquids, Mg nanoparticles with thin oxide layers, MgO HNPs, and pure MgO nanocubes were produced, respectively (Figure 3f–j and Table 1). Pure *n*-hexane was expected to prevent the pure Mg nanoparticles from fast oxidation during the LAL process, and the thin oxide layer, as seen in Figure 3g, could form because of water traces in hexane and/or during the preparation and observation of the TEM sample. The HNPs appeared in the liquid medium with moderate oxidizing potential, where Mg/MgO core/shell particles were expected to form first and then immediately turn into HNPs. Finally, in the most oxidizing liquid, the ablated metal particles were likely to be immediately oxidized to the MgO nanocubes observed in Figure 3i,j. Therefore, the MgO HNP preparation also proves their formation via the Kirkendall process.

Besides the HNPs, one-step laser ablation of metal targets also led to core/shell nanoparticles (Figure 4a,d,g). They appeared in the Kirkendall systems with a low diffusibility of metal ions in the shells<sup>22,23</sup> (Zn/O and Ti/O) or where the oxidation of metal cores by the liquid medium was too deep, causing shells to be too thick (Pb/S, dodecyl mercaptan/*n*-hexane medium). The Kirkendall process in these two cases was believed not to proceed fast

(33) Fan, H. J.; Knez, M.; Scholz, R.; Hesse, D.; Nielsch, K.; Zacharias, M.; Gosele, U. *Nano Lett.* **2007**, *7*, 993–997.

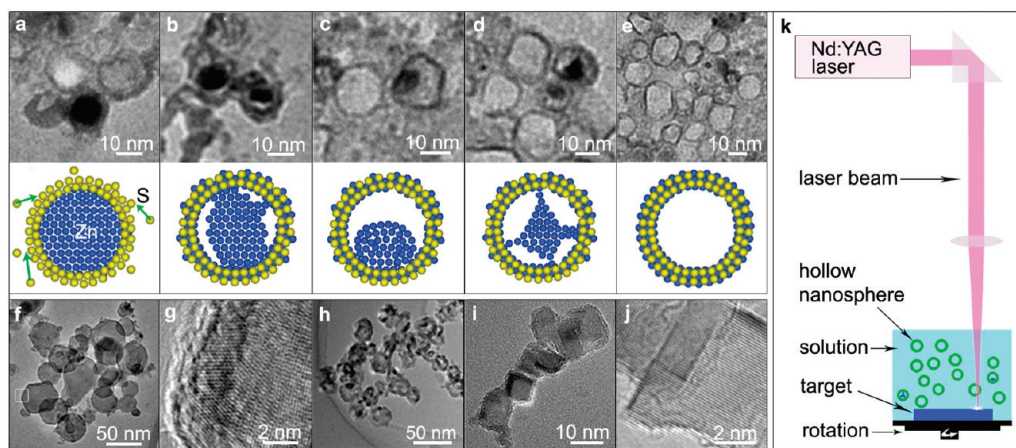


**Figure 3.** TEM images of products of one-step laser treatment in different systems. (a–e) ZnS HNPs found at different stages of formation and the corresponding structural models. (f) Mg/MgO core/shell nanospheres obtained in an *n*-hexane medium. (g) HRTEM of the particle edge from image f. (h) MgO HNPs obtained in an *n*-hexane/ethanol medium. (i) MgO nanocubes obtained in an ethanol medium. (j) HRTEM of a particle from image i. (k) Scheme of the setup used to prepare HNPs via the Kirkendall effect (one-step laser treatment).

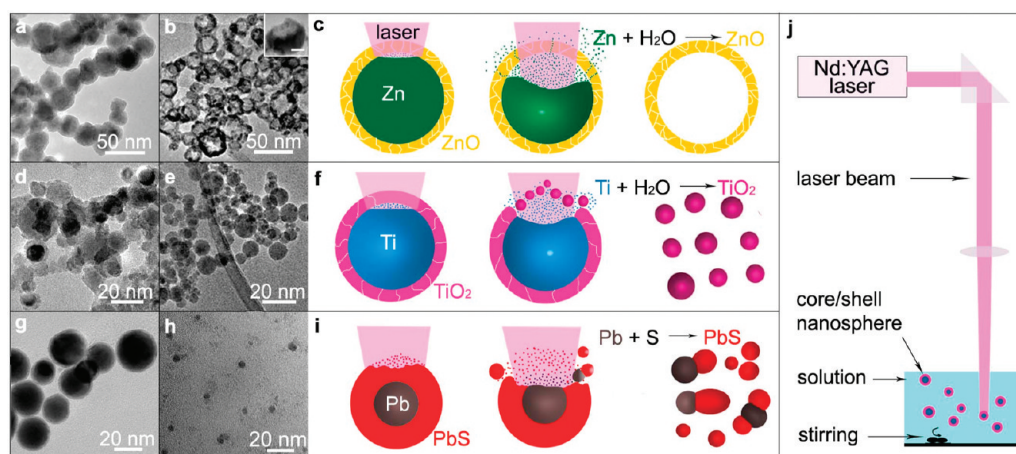


**Figure 4.** Effect of second-step laser treatment in three different systems. (a) TEM image of Zn/ZnO core–shell nanospheres after one-step laser treatment. (b) TEM image of ZnO HNPs after second-step laser treatment. The inset shows a TEM image of a partially vaporized Zn core in a ZnO shell during HNP formation, where the scale bar is 10 nm. (c) Scheme of selective core vaporization by laser and product formation in this system during second-step laser treatment. (d) TEM image of Ti/TiO<sub>2</sub> core/shell nanospheres after one-step laser treatment. (e) TEM image of smaller TiO<sub>2</sub> nanospheres after second-step laser treatment. (f) Scheme of TiO<sub>2</sub> shell destruction by Ti vapor in this system. (g) TEM image of Pb/PbS core/shell nanospheres after one-step laser treatment in dodecyl mercaptan/*n*-hexane. (h) TEM image of Pb–PbS hybrid nanostructure after second-step laser treatment. (i) Scheme of PbS shell destruction by laser in this system. (j) Setup used for the second-step laser treatment.

enough, and the metal cores remained (visually or partially) intact because of the short laser pulse duration and the strong quenching effect during subsequent cooling. Some of these core/shell structures produced by one-step laser ablation could be further converted into HNPs by employing selective-laser vaporization as an additional step. When a laser with a given wavelength irradiates appropriate metal-core/shell nanospheres, the cores can be vaporized by the laser, leaving the laser-transparent shells unchanged and thus producing HNPs. Such a selective-vaporization approach intuitively needs two prerequisites from the nanostructures to be treated. First, the melting point of the shell should be higher than the boiling point of the core so that the shell is not damaged by the laser-induced metal vapor. Second, the band gap of the shell must be larger than the laser photon energy; otherwise, the shell can be heated and destroyed by the laser irradiation.

According to the physical constants listed in Supporting Information Table S1, the core/shell nanostructure of Zn/ZnO meets both requirements and ZnO HNPs were indeed obtained

after a second-step laser treatment (Figure 4a–c). For the Ti/TiO<sub>2</sub> system, the melting point of the TiO<sub>2</sub> shell is lower than the boiling point of the Ti core; therefore, the TiO<sub>2</sub> shell was expected to be destroyed by Ti vapor, and further reaction of Ti vapor with water resulted in TiO<sub>2</sub> nanoparticles (Figure 4e,f). For the Pb/PbS system, the energy band gap of PbS (0.14 eV) is lower than the laser photon energy used (1.17 eV), hence the PbS shell could absorb the laser energy and be heated and destroyed, giving rise to the Pb–PbS hybrid nanostructures and PbS nanoparticles seen in Figure 4h,i. The above results indicate that the selective laser vaporization of core/shell nanostructures is also an efficient way to produce HNPs by processing certain core/shell nanoparticles. It is more practical than thermal incubation and electron beam irradiation approaches,<sup>19,21</sup> which were also used successfully to convert core/shell particles into their corresponding HNPs (Supporting Information Figure S3). This technique is very simple and is believed to be potentially applicable to other material systems, including Cd/CdS and Cd/CdO, where CdS and CdO HNPs are expected upon laser treatment.

Because of the peculiarities and discontinuity of laser pulses, the LAL method possesses such characteristics as high local processing temperatures, high heating rates, and high cooling rates.<sup>27,34</sup> Hence, the formation of HNPs through this method exhibits several unique features. First, a one-step synthesis process is possible in many systems, being very simple and productive. The preparation of HNPs through the Kirkendall effect via conventional chemical routes usually requires four stages: the synthesis of metal nanoparticles, the formation of a compact compound layer on the metal cores, the separation of the core and shell through the Kirkendall effect, and the diffusion of the metal core for voiding.<sup>17,33</sup> Each of the steps needs precise control and a rather long reaction time.<sup>17</sup> In our approach, the HNP formation can be accomplished after just one laser pulse. The synthesis time is thus ultrashort, and the HNP type can be conveniently defined by varying the target and the liquid medium. Second, HNPs made from reactive metal oxides can be synthesized by this process. In common chemical routes, nanoparticles of such metals are hard to prepare because of their high reactivity. A pulsed laser can provide a high power density for heating and ablating the target rapidly, after which a cold liquid medium quenches the high-temperature phase into metal particles. The transformation is so quick that, in a proper liquid medium, oxidation cannot proceed far and therefore even very reactive metal nanoparticles (covered with an oxide shell) can be produced, immediately giving rise to related HNPs via the Kirkendall process during the very same quenching phase. Third, the method described here is environmentally friendly compared to the majority of conventional chemistry routes presently exploited. It is a one-pot approach and can use minimum quantities of chemical reagents, which serve both as a liquid medium and an oxidizer.

HNPs are usually considered to be very effective gas-sensing materials because of their large surface-to-volume ratio.<sup>2</sup> Hence, we investigated one type of prepared HNP (ZnS) as a potential gas sensors for acetone and ethanol. The sensing device based on the ZnS HNPs is seen in Figure 5a to exhibit very short response and recovery times (about 3 s) for both of the detected gases. The external resistance shows a stepped change with the concentration of the detected gases (Figure 5b), and the sensitivity of the devices (defined as  $S = R_a/R_g$ , where  $R_a$  is the device resistance in air and  $R_g$  is its resistance in the presence of a detected gas) increases linearly with the concentration (Figure 5c), which makes such devices very practical. For comparison, a similarly assembled device with ZnS nanocrystals showed a significantly lower sensitivity to ethanol gas when operated under similar conditions (Supporting Information Figure S4).

According to the space-charge region model,<sup>35</sup> as the sensor is exposed to air, the electrons in the sensing material can be extracted by the adsorbed oxygen molecules, leading to a narrow conduction channel and high electrical resistance. In contrast, when the sensor is exposed to reducing gases, the trapped electrons will be released owing to reactions between reducing gases and adsorbed oxygen molecules, and then the conduction channel becomes wider, giving rise to a lower electrical resistance.<sup>35</sup> Theoretically, the rate of the surface reaction is proportional to the number of available adsorption sites on the surface of a nanostructure.<sup>36</sup> Considering the extreme synthesis conditions generated by a laser pulse, numerous

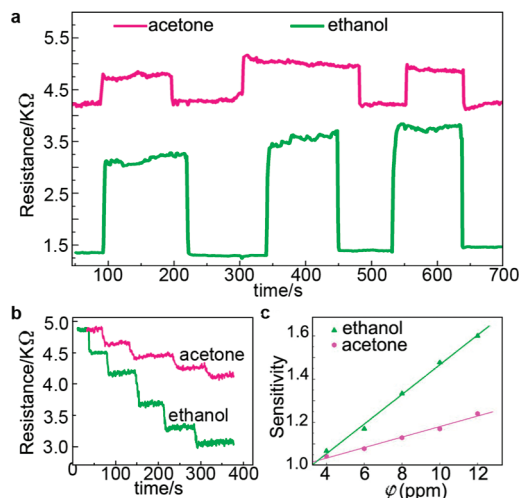


**Figure 5.** Gas-sensing properties of ZnS HNPs. (a) Response and recovery curves of the sensing device built from ZnS HNPs. The concentrations of acetone and ethanol are 4 and 100 ppm, respectively, and the working voltage is 7 V. (b) Stepped decrease in resistance values ( $R_g$ ) for a continuous time, with a 2 ppm increment of gas concentration ( $\phi$ , volume fraction) in each step. (c) Sensitivity vs concentration curves for the ZnS HNP-based device as acetone and ethanol sensors.

defects could be produced in the ZnS HNPs, which then serve as adsorption sites and are thus responsible for the enhanced sensitivity of the HNPs to detected gases.

Surface defects, such as dangling sulfur bonds, were reported to generate unpaired electrons, which causes ferromagnetism through the exchange interaction.<sup>37,38</sup> In our previous report (ref 29, Figure 7e,f), we compared the magnetic behavior of ZnS HNPs and ZnS nanocrystals at two different temperatures (5 and 305 K). Both the ZnS HNPs and ZnS nanocrystals were shown to exhibit ferromagnetism with nonlinear curves and a hysteresis loop at 5 and 305 K, but the saturation magnetization of the HNPs was about 2 times larger than that of their nanocrystal counterparts.<sup>29</sup> Considering the higher surface-to-volume ratio of the HNPs, the higher saturation magnetization can be ascribed to more surface-related defects in the hollow structures. Therefore, the results of magnetic measurements presented in ref 29 are consistent with the above explanation of the superior gas-sensing properties of the ZnS HNPs resulting from numerous surface-related defects on these hollow structures. Besides, the hollow, porous structure is obviously more favorable to the diffusion, absorbance, and desorbance of gas molecules than the compact structure of nanocrystals. Thus, the electrical resistance of HNPs should change significantly in different gas environments. These two factors are jointly believed to cause the excellent gas-sensing properties of the ZnS HNPs observed.

## Conclusions

Laser ablation in a liquid is proven to be a fast, versatile synthesis route for preparing ultrafine hollow nanospheres in many systems. Two mechanisms were responsible for the formation of HNPs prepared in this study. The Kirkendall effect led to HNPs in the systems with fast enough metal diffusivity in their oxide/sulfide shell, and selective laser vaporization of the metal core by an IR laser was applied as a second-step treatment in the systems with slower metal diffusivity in the shell. Because of the unique dynamic features of the

(34) Qin, W. J.; Kulnich, S. A.; Yang, X. B.; Sun, J.; Du, X. W. *J. Appl. Phys.* **2009**, *106*, 114318.

(35) Scott, R. W. J.; Yang, S. M.; Chabanis, G.; Coombs, N.; Williams, D. E.; Ozin, G. A. *Adv. Mater.* **2001**, *13*, 1468–1472.

(36) Zhang, J.; Wang, S. R.; Xu, M. J.; Wang, Y.; Zhu, B. L.; Zhang, S. M.; Huang, W. P.; Wu, S. H. *Cryst. Growth Des.* **2009**, *9*, 3532–3537.

(37) Sundaresan, A.; Rao, C. N. R. *Nano Today* **2009**, *4*, 96–106.

(38) Sundaresan, A.; Bhargavi, R.; Rangarajan, N.; Siddesh, U.; Rao, C. N. R. *Phys. Rev. B* **2006**, *74*, 161306.

LAL process, the products were expanded to new systems and uncommon HNPs (such as MgO and PbS) were prepared. ZnS HNPs were tested as gas sensors and demonstrated superior performance. This method is believed to serve as a versatile and universal technique for achieving various nanostructures. By adjusting the target and the liquid medium, various nanostructures can be achieved, such as core/shell nanospheres, heterostructures, and compound nanospheres. The process can thus endow more new products with specific properties that are waiting for fabrication and study.

**Acknowledgment.** This work was supported by the Natural Science Foundation of China (nos. 50972102 and 50902103) and the National High-tech R&D Program of China (nos. 2007AA021808 and 2009AA03Z301)

**Supporting Information Available:** Experimental details and structural characterization of the as-produced nanostructures. This material is available free of charge via the Internet at <http://pubs.acs.org>.